Indian Journal of Pure & Applied Physics
Vol. 60, July 2022, pp. 561-566

External Perspective of Lung Airflow Model Through Diaphragm Breathing Sensor Using Fiber Optic Elastic Belt

Defrianto[a], Toto Saktioto[a]*, Nurfi Hikma[a], Yan Soerbakti[a], Dedi Irawan[b], Okfalisa[c], Bambang Widiyatmoko[d] & Dwi Hanto[d]

[a]Department of Physics, Mathematics and Natural Sciences, Universitas Riau, Pekanbaru, 28293, Indonesia

[b]Department of Physics Education, Teacher Traning and Education, Universitas Riau, Pekanbaru, 28293, Indonesia

[c]Department of Informatics Engineering, Science and Technology, Universitas Islam Negeri Sultan Syarif Kasim, Pekanbaru, 28293, Indonesia

[d]Research Center of Physics, National Research and Innovation Agency PUSPIPTEK Serpong, South Tangerang, 15314, Indonesia

Received 14 April 2022; accepted 17 June 2022

Optical fiber-based detector technology is highly appreciated and developed in the field of medical physics. Through its fiber-optic wave pattern performance, this detector has great potential for monitoring difficult-to-calculate parameters such as airflow in the lungs. To realize this reality, a theoretical and experimental approach is needed in this research. The lung tissue model was formed using the Navier-Stokes equation using the finite element method by taking into account the continuity and momentum equations. While experimentally, single-mode fiber and fiber Bragg grating (FBG) was installed with a sinusoidal macro bending pattern as a strain sensor which was applied to the elastic belt and mounted on the diaphragm. The simulation model carried out depicts the velocity of air moving from the pulmonary duct to increase as it flows into smaller branches. While the experimental results show that the detected power parameter is a maximum of -0.16 dBm during inhalation and a minimum of -0.19 dBm during expiration. Due to the bending approach, the FBG sensor belt obtained the highest sensitivity at a sinusoidal bending diameter of 0.8 cm. Therefore, this is good news as a more accurate detector approach for medical purposes.

Keywords: Fiber optic sensor; Fiber Bragg grating; Respiratory; Navier-Stokes; Sinusoidal bending

1 Introduction

The development of the modern industrial revolution is advancing because of the many innovations in fiber optic sensor (FOS) technology that play an important role in various scientific fields. Micro-thin FOS have the ability to transmit signals over long distances with high bandwidth and transfer rates (up to gigabits per second). In addition, optical fiber is also immune to electromagnetic interference and low fabrication costs[1,2]. Therefore, fiber optic technology shows wide application, both in telecommunications and other fields including medical science, in terms of monitoring human organ signals.

There are four dominant signs in humans that can be detected by fiber optic technology, namely body temperature, pulse or heart rate, breathing, and blood pressure[3]. The current main indication that can be applied to fiber optic detection objects is the lung organ. Consequently, respiratory monitoring can identify lung disease, including renal failure, stroke, and apnea[4]. Currently, breathing sensors in conventional electronic form are judged to be only able to measure the rise and fall of the chest cavity. However, it is not very sensitive to distinguish between shallow breathing (tachypnea) and cessation. In addition, the use of conventional electronic sensors carries the risk of sticking directly to the body, which can cause irritation and discomfort to the skin[5].

Strain-sensitive single-mode fiber (SMF) and fiber Bragg grating (FBG) devices show great potential for the development of lung respiratory signal sensor technology[6,7]. The use of SMF and FBG as detectors has several advantages over other types of sensors, including micro-scale fiber size, resistance to electromagnetic interference, high precision, and easy modification with non-obstructive composite materials[8,9]. There is a FOS design pattern that is commonly applied in monitoring, namely sinusoidal, straight, and U configuration patterns[10]. However, several previous studies have shown that the sinusoidal patterned optical fiber is the most effective in detecting changes in parameters in the human body[11]. Therefore, the use of sinusoidal patterns in SMF and FBG provides high potential for response analysis on human

*Corresponding authors: (Email: saktioto@lecturer.unri.ac.id)

diaphragmatic breathing activity. The FOS technology developed in this study has a belt form consisting of a sinusoidally configured SMF and FBG. The sensitivity value of the FOS can be obtained by calculating the power losses from variations in the diameter of the sinusoidal pattern and abdominal circumference in men and women as experimental samples.

Although the investigation of demonstration fiber-optic biosensors has shown good progress, current theoretical models and simulation approaches are also considered to have new information for certain cases such as fluid mechanics of airflow, heat distribution, and viscosity. So airflow modeling in human breathing has an important role in validating and comparing with experiments. Therefore, this paper discusses the theoretical approach of simulation and experimentation to explain the phenomenon of airflow vibration for diaphragmatic breathing.

2 Theoretical Consideration

The light pulses are sent by the optical fiber from one place to another through the medium (core) by bouncing off the cladding. This is due to perfect reflection (no light is refracted), and is represented in Equation (1)[12],

$$\Delta = \frac{n_1^2 - n_2^2}{2n_1^2} = \frac{n_1 - n_2}{n_1} \quad \ldots (1)$$

where the refractive index of optical fiber consists of n_1 (core) and n_2 (cladding), and Δ is the difference in the refractive index of cladding and core.

The mode theory is based on the optical fiber type that views light as a waveform. This concept is expressed in terms of the direction, amplitude, and wavelength (λ) of the propagation path given by[13],

$$\lambda = \frac{c_o}{nf} \quad \ldots (2)$$

where c_o is the speed of light in a vacuum (3×10^8 m/s), n is the medium refractive index, and f is the light frequency (Hz), with several modes calculated by the following[14],

$$M_{FO} = \frac{1}{2}\left(\frac{\pi D_f NA}{\lambda}\right)^2 \quad \ldots (3)$$

where M_{FO} is a number of generated modes, D_f is the core diameter (m), dan NA is the numeric level. Furthermore, the FBG-based sensor has a Bragg lattice that produces light waves that are reflected and also transmitted in the optical fiber without any changes. These devices reflect a number of wavelengths of light and transmit the rest due to the addition of periodic variations in the refractive index of the core.

Optical fiber losses are caused by three main factors, namely Rayleigh dispersion, buckling, coupling mode losses, and splicing and material. This study discusses buckling losses due to macro-bending activities which by definition can be expressed as the difference between unbending fiber losses and bent fiber losses or in other expressions as[15],

$$L = 10\, log\left(\frac{P_f}{P_i}\right) \quad \ldots (4)$$

where L is power loss (dB), P_f is final power (dBW), dan P_i is initial power (dBW). When the angle of incidence is smaller than the critical angle, the mode of light cannot be perfectly reflected[16], but is refracted out of the optical fiber core. If the angle is small, it will be reflected back into the casing and a total reflection occurs. The optical radiation from the curvature formed will be greatly influenced by the diameter treatment.

FOS has introduced several methods and devices based on fiber optic which are useful for monitoring heart rate and respiration[17]. In addition, the configuration used in FOS consists of several configurations, and the most frequently applied is the Fabry Perot Interferometer on invasive sensors. The bending method can cause light coupling from the directional mode to the radiation mode. The use of an elastic substrate and a sinusoidal pattern in this sensor makes the period of change of the bent fiber change with the action of breathing and heart rate. Furthermore, the periodicity variance of the bent fiber will be transformed into a change in the amplitude of the fiber structure.

3 Materials and Methods

This study discusses the model and demonstration of diaphragmatic breathing that produces airflow vibrations. A model of respiratory flow to the lungs is theoretically based on the Navier Stokes Equation. The model used by this equation is carried out by the finite element method. The equations consist of continuity and momentum equations for incompressible fluids. Navier-Stokes are formed as follows[18]:

– Continuity

$$\frac{\partial U}{\partial x} + \frac{\partial V}{\partial y} + \frac{\partial W}{\partial z} = 0(5) \quad \ldots (5)$$

– X-momentum

$$\rho\left(\frac{\partial U}{\partial t}+U\frac{\partial U}{\partial x}+V\frac{\partial U}{\partial y}+W\frac{\partial U}{\partial z}\right)=-\frac{\partial P}{\partial x}+\rho g_x+\mu\left(\frac{\partial^2 U}{\partial x^2}+\frac{\partial^2 U}{\partial y^2}+\frac{\partial^2 U}{\partial z^2}\right) \quad \ldots (6)$$

– Y-momentum

$$\rho\left(\frac{\partial V}{\partial t}+U\frac{\partial V}{\partial x}+V\frac{\partial V}{\partial y}+W\frac{\partial V}{\partial z}\right)=-\frac{\partial P}{\partial y}+\rho g_y+\mu\left(\frac{\partial^2 V}{\partial x^2}+\frac{\partial^2 V}{\partial y^2}+\frac{\partial^2 V}{\partial z^2}\right) \quad \ldots (7)$$

– Z-momentum

$$\rho\left(\frac{\partial W}{\partial t}+U\frac{\partial W}{\partial x}+V\frac{\partial W}{\partial y}+W\frac{\partial W}{\partial z}\right)=-\frac{\partial P}{\partial z}+\rho g_z+\mu\left(\frac{\partial^2 W}{\partial x^2}+\frac{\partial^2 W}{\partial y^2}+\frac{\partial^2 W}{\partial z^2}\right) \quad \ldots (8)$$

where U, V, and W are the air flow speed over the x, y and z coordinate. The value of P is pressure, ρ is fluid density and μ is viscost.

This model of airflow in the direction of breathing is arranged in three dimensions of flow as a resonator forms and branches to the lungs. This finite element model is designed as a tissue of elements as depicted in Figs 1 (a & b). Respiratory airflow modelling represents 2D in the branch to the lungs. This model is designed to connect the trachea which connects to the left and right bronchi and then connects to the bronchioles, which are smaller bronchi. The diameter and length of the trachea were 1 cm and 10 cm, respectively, where the diameter and length of the bronchi were 0.5 cm and 4 cm and the diameter and length of the bronchioles were 0.2 cm and 1 cm, respectively. A set of tissue element models has a size of 0.01 cm.

Design and operation of diaphragmatic breathing airflow vibrations were experimentally regulated and measured with an optical biosensor using an FBG as shown in Fig. 2. The interior of the belt contains SMF and FBG optical fibers with a wavelength of 1310 nm and a power source of -5 dB, in a sinusoidal pattern characterized by marked with a diameter (X) alternating 0.8 cm and 1.2 cm, respectively. In addition, the power source comes from the laser diode, while the input and output power is detected by the optical power meter due to its maximum displacement (A) during respiration when the belt is fastened to the diaphragm section.

The experimental sample consisted of seven people with variations in abdominal circumference (near the diaphragm) of 64, 66, 69, 72, 77, 83, and 97 cm. However, the ages of the individuals did not differ significantly and were in the range of 21 to 23 years. While the standing / upright position looks correct with normal breathing conditions, without previous physical activity. The next generation is monitored every second for 60 seconds in 5 repetitions. The resulting data graph is used to calculate the frequency/number of breaths in 1 minute. Then the rhythm and pattern of breathing are formed, followed by analyzing the effect of the output power on the abdominal circumference from loss of power. This power loss calculation is used to determine the sensitivity level of several types of sinusoidal pattern diameters.

4 Results and Discussion

The airflow model simulation is depicted in Fig. 3 by setting and entering parametric values, namely air density 1.225 kg/m^3, viscosity 1.7894 × 10^{-5} kg/m.s, and air velocity 1 m/s. In the first branch, the airflow velocity is 1.5 m/s, and then it increases by a factor of 2 m/s above the initial input velocity. As the airflow moves to the second branch, its velocity increases further from 3.5 m/s to 4 m/s. This explains that the mechanical strength of air and fluid parameters affect the airflow in the lung passages. Air density contributes more to air velocity than viscosity. It seems that the air discharge has the same value for each lung branch.

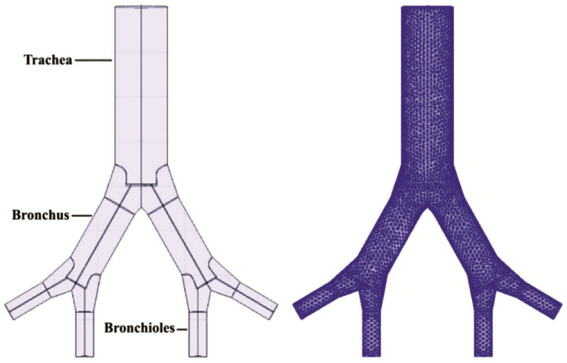

Fig. 1 — Airflow model to the lungs (left) and a finite element model of the lungs in 2D (right).

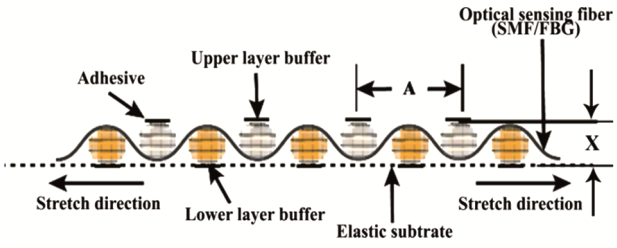

Fig. 2 — Display of sinusoidal pattern FOS micro bends within the belt.

Experimentally, the value of the input power was measured with an optical power meter (OPM) in a straight-line position. The input power for SMF and FBG with diameters of 0.8 and 1.2 cm is -6.32 dBm and -7.16 dBm, and -6.58 dBm and -7.34 dBm, respectively. Next, the end of the fiber with the connector is connected to the laser diode and the OPM. The experimental sample is in an upright position and normal breathing is monitored then the output power is measured on the device for every second at 1-minute intervals. In addition, the first 60 seconds for the first object are recorded as the first try and this process is repeated for 5 minutes to reach the 5th attempt, before moving on to the next object. However, every 60 seconds, the belts were reconditioned to maintain the same treatment between trials. In general, the change in power is obtained by Equation (9)[19],

$$\Delta P = P_f - P_i \quad \ldots (9)$$

where ΔP is is the change in power (dBm) calculated after the FOS belt is installed in the first sample and the results can be seen in Fig. 4.

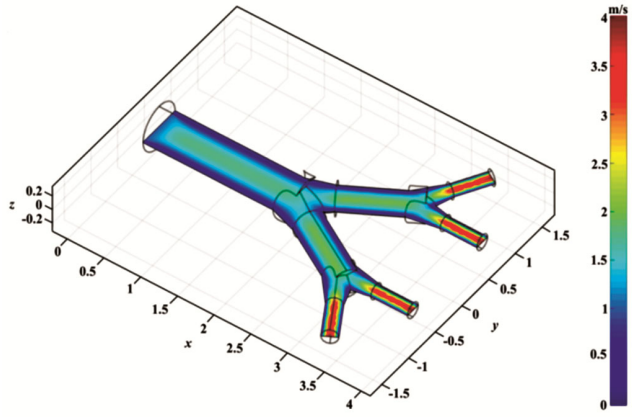

Fig. 3 — Air flow speed with various branch sizes to the lungs in 3D.

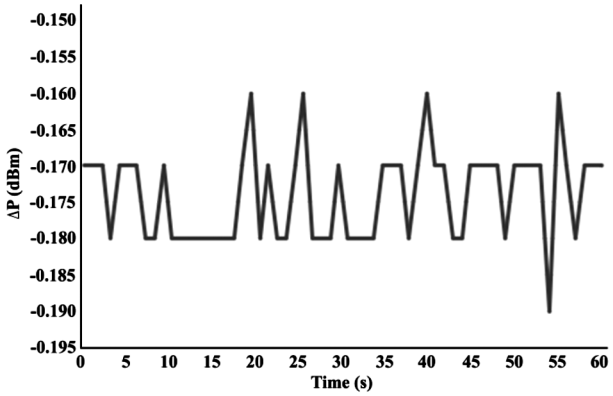

Fig. 4 — SMF power change oscillation for diameter 1.2 cm in the first sample for 60 seconds.

As depicted in Fig. 4, Oxygen (O_2) is inhaled as the curve moves up, while Carbon Dioxide (CO_2) is exhaled for a downward movement. Further maximum peaks were observed at 19, 26, 40, and 55 seconds. Inhalation also occurs in the seconds before and after, albeit at a slightly higher peak. This represents the respiratory difference and when calculated, the total inhalation and exhalation peak is 13, corresponding to the number of human apneas (a measure of frequency) in the range of 12 to 20 breaths per minute[20].

Figure 5 is the distribution for the combined respiratory outcomes. If the SMF value for diameter 1.2 cm occurs in the range of -0.20 to -0.30 dBm or with a change of -0.10 dBm, then the FBG results are obtained at the same diameter. These results indicate the presence of varying degrees of sensitivity, with separate distributions of data outside the normal range. At the same gray point (Exp.3), the data distribution is in the range of -0.10 to -0.30 dBm, between 1st and 28th seconds. However, different results were also obtained for the yellow color point (Exp.4) with a higher value, compared to the gray point (Exp.3) of -1.20 to -1.50 dBm. Meanwhile, mixed experimental results are reported in the normal radian range.

Based on various distributions of data, a range of values was obtained, without physical activity which was not under normal conditions for this study. The minimum and maximum power are derived and then the median value is evaluated. As a result, smaller abdominal circumferences tend to produce a fairly large median power, and vice versa with more negative results. Furthermore, power losses are closely related to changes in power as written in Equation (9) and described in Fig. 6.

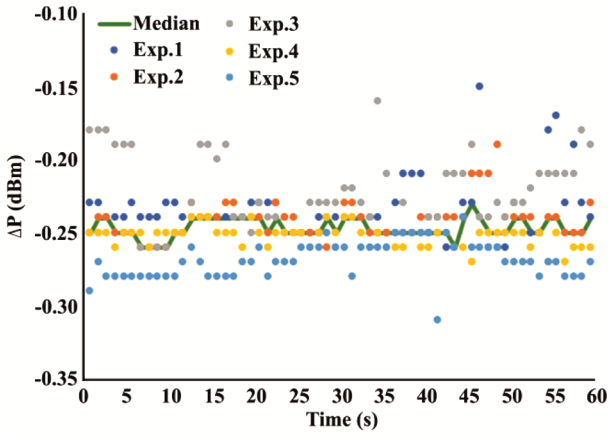

Fig. 5 — FBG vibration pattern for diameter 1.2 cm in the second experimental sample.

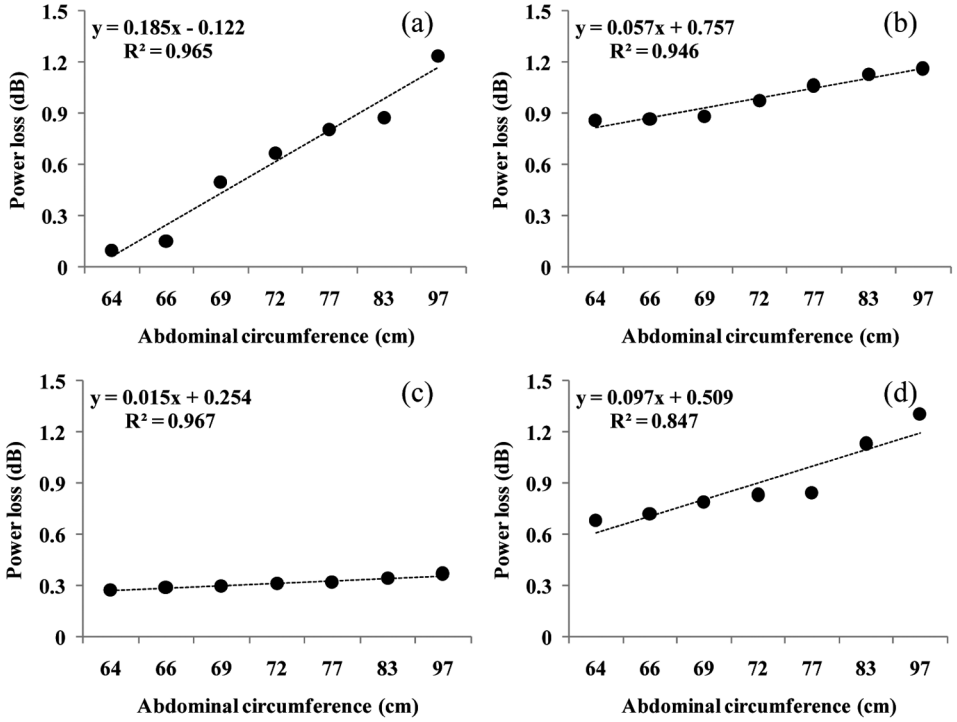

Fig. 6 — Power loss function on SMF with (a) X = 1.2 cm, (b) X = 0.8 cm and FBG with (c) X = 1.2 cm, (d) X = 0.8 cm.

Figure 6 illustrates the power loss with a practical linear curve. Therefore, a larger abdominal circumference results in a smaller median force and a higher power loss value. While the power loss tends to be significant, with a reduced diameter. In particular, the large value of power loss occurs in the sinusoidal pattern of diameter 0.8 cm in both SMF and FBG. Currently, by observing the two types of optical fiber, FBG is known to produce the maximum estimate. However, in the initial object, a high power loss value for diameter 0.8 cm is present in SMF, but the highest peak is observed in FBG at the same diameter. These results are consistent with previous studies[4], where power loss tends to increase as the diameter of the sinusoidal pattern decreases. Therefore, to describe the power losses, the sensitivity is evaluated using the output power approach as follows [21],

$$S = \frac{P_2}{P_1} = \frac{\Delta P_m}{P_i} = \frac{P_m - P_i}{P_i} \quad \ldots (10)$$

The minimum diameter appears to be more sensitive, compared to the larger diameter as shown in Table 1. A similar study in FOS also reported a broad sensitivity, using a lower diameter[22]. In addition, the application of a sinusoidal pattern with 3 variations in diameter 3, 4, and 8 cm, obtained sensitivity values of 0.1171, 0.0904, and 0.0657 V/cm, respectively. Furthermore, the small-diameter optical fiber of the test membrane tends to trigger the angular reception of the light by the optical fiber as a receiver at a numerical aperture value[23].

Table 1 — FOS belt sensitivity values for SMF and FBG in each experimental sample.

Abdominal circumference (cm)	FOS belt sensitivity			
	SMF		FBG	
	X = 1.2 cm	X = 0.8 cm	X = 1.2 cm	X = 0.8 cm
64	0.0223	0.2183	0.0646	0.1702
66	0.0349	0.2199	0.0686	0.1808
69	0.1215	0.2246	0.0713	0.1990
72	0.1662	0.2515	0.0740	0.2112
77	0.2039	0.2768	0.0767	0.2142
83	0.2234	0.2958	0.0821	0.2978
97	0.3296	0.3069	0.0888	0.3495

However, a certain variation with a sensitivity that is more similar to the first experimental sample, was observed for the SMF value 0.306962 at diameter 0.8 cm. This estimate appears to be larger, compared to FBGs at equivalent diameters, although various factors may be involved, including the placement of the Bragg lattice. Therefore, to be more effective, the calculated sensitivity value is calculated with the resulting power losses. In addition, the FBG power

loss value for diameter 0.8 cm showed a clearer difference between samples, with a higher range of values, compared to SMF at the same diameter. As a result, the most sensitive and effective performance occurred in FBG at diameter 0.8 cm.

5 Conclusions

During diaphragmatic breathing, the characteristics of the respiratory airflow have been successfully tried and modeled. Airflow varies with the respiratory flow as a function of channel geometry where velocity increases from 1.5 m/s to 4 m/s as it moves to smaller branch sizes. Airflow velocity is more affected by density than viscosity and airflow rate is almost the same for each branch. Experimentally, the variation of the strain sensor in the diameter of the sinusoidal pattern for all samples produced different results for the frequency and number of breaths, in terms of the vibrational pattern of diaphragmatic breathing. The sensitivity of SMF and FBG for a diameter of 0.8 cm appears to be greater than that of 1.2 cm. Furthermore, increasing the FBG value is considered to be more effective than the SMF estimation.

Acknowledgments

The authors are grateful to The Ministry of Education, Research and Technology, Indonesia, for the research Grant's generous support in 2022. Furthermore, the authors are grateful to the Department of Physics, Mathematics and Natural Sciences Faculty, and LPPM Universities Riau, Pekanbaru Indonesia for providing research facilities.

References

1 Yang Y, Hong C, Abro Z A, Wang L & Yifan Z, *Sens Actuators A*, 295 (2019) 663.
2 Saktioto T, Ramadhan K, Soerbakti Y, Syahputra R F, Irawan D & Okfalisa, *Telkomnika*, 19 (2021) 1982.
3 Kebe M, Gadhafi R, Mohammad B, Sanduleanu M, Saleh H & Al-Qutayri M, *Sensors*, 20 (2020) 1454.
4 Inan O T, Etemadi M, Wiard R M, Giovangrandi L & Kovacs G T A, *Physiol Meas*, 30 (2009) 169.
5 Yang X, Chen Z, Elvin C S M, Janice L H Y, Ng S H, Teo J T & Wu R, *IEEE Sens J*, 15 (2014) 757.
6 Saktioto T, Ramadhan K, Soerbakti Y, Irawan D & Okfalisa, *J Phys: Conf Ser*, 2049 (2021) 012001.
7 Saktioto T, Fadilla F D, Soerbakti Y, Irawan D & Okfalisa, *J Phys: Conf Ser*, 2049 (2021) 012002.
8 Zhao Y, Li X G, Zhou X & Zhang Y N, *Sens Actuators B*, 231 (2016) 324.
9 Saktioto, Zairmi Y, Veriyanti V, Candra W, Syahputra R F, Soerbakti Y, Asyana V, Irawan D, Okfalisa, Hairi H, Hussein N A, Syamsudhuha & Anita S, *J Phys: Conf Ser*, 1655 (2020) 012160.
10 Yang M, Liu Q, Naqawe H S & Fok M P, *Sensors*, 20 (2020) 1312.
11 Drissi-Habti M, Raman V, Khadour A & Timorian S, *Sensors*, 17 (2017) 667.
12 Vigneswaran D, Rajan M M, Ayyanar N & Patel S K, *Optik*, 228 (2021) 169040.
13 He Y, Zhang X, Zhu L, Sun G, Lou X & Dong M, *Sensors*, 19 (2019) 2727.
14 Abaie B, Peysokhan M, Zhao J, Antonio-Lopez J E, Amezcua-Correa R, Schülzgen A & Mafi A, *Optica*, 5 (2018) 984.
15 Saktioto T, Dewi S P, Syahputra R F, Okfalisa O & Syamsudhuha S, *Telkomnika*, 17 (2019) 2194.
16 Farmani A & Mir A, *IEEE Photonics Technol Lett*, 31 (2019) 643.
17 Roriz P, Carvalho L, Frazão O, Santos J L & Simões J A, *J Biomech*, 47 (2014) 1251.
18 Ershkov S V, *Int J Fluid Mech Res*, 42 (2015) 206.
19 Zaca-Morán P, Padilla-Martínez J P, Pérez-Corte J M, Dávila-Pintle J A, Ortega-Mendoza J G & Morales N, *Laser Phys*, 28 (2018) 116002.
20 Liu L, Shah S A, Zhao G & Yang X, *Appl Sci*, 8 (2018) 568.
21 Fu Y & Di H, *Opt Laser Technol*, 43 (2011) 586.
22 Fukano H, Aiga T & Taue S, *Jpn J Appl Phys*, 53 (2014) 04EL08.
23 Li M, Nyayapathi N, Kilian H I, Xia J, Lovell J F & Yao J, *Mol Imag*, 19 (2020) 22.